Phenoxyl Radical Complexes of Zinc(II)

Achim Sokolowski, Jochen Müller, Thomas Weyhermüller, Robert Schnepf, Peter Hildebrandt, Knut Hildenbrand, Eberhard Bothe, and Karl Wieghardt*

Contribution from the Max-Planck-Institut für Strahlenchemie, P.O. Box 10 13 65, D-45413 Mülheim an der Ruhr, Germany

Received February 7, 1997[⊗]

Abstract: A series of phenoxyl radical complexes of zinc(II) have been generated in solution and, in one instance, isolated as solid material (**5**) in order to study their spectroscopic features by EPR, resonance Raman, and UV−vis spectroscopy. They serve as model complexes for the active form of the copper containing fungal enzyme galactose oxidase. The complexes $[Zn(L^1H_2)]BF_4 \cdot H_2O$ (**1**), $[Zn(L^2H_2)]BF_4 \cdot H_2O$ (**2**), $[Zn(L^2H)]$ (**2a**), $[Zn(L^3)(Ph_2acac)]$ (**3**), $[Zn(L^4)(Ph_2acac)]$ (**4**), and $[Zn(L^4)(Me\text{-}acac)]$ (**6**) were synthesized from solutions of $Zn(BF_4)_2 \cdot 4H_2O$ and the corresponding ligand (L^1H_3 = 1,4,7-tris(3,5-*tert*-butyl-2-hydroxybenzyl)-1,4,7-triazacyclononane; L^2H_3 = 1,4,7-tris-(3-*tert*-butyl-5-methoxy-2-hydroxybenzyl)-1,4,7-triazacyclononane; L^3H = 1,4-dimethyl-7-(3,5-di-*tert*-butyl-2-hydroxybenzyl)-1,4,7-triazacyclononane; L^4H = 1,4-dimethyl-7-(3-*tert*-butyl-5-methoxy-2-hydroxybenzyl)-1,4,7-triazacyclononane, Ph_2acac^- = 1,3-diphenyl-1,3-propanedionate, and Me-$acac^-$ = 3-methyl-2,4-pentanedionate). Complexes **2**, **3**·0.5 toluene·1n-hexane, and **4** were structurally characterized by single-crystal X-ray crystallography. An electrochemical investigation of these complexes in CH_3CN and/or CH_2Cl_2 solution revealed that the coordinated phenolate ligands undergo reversible one-electron oxidations with formation of coordinated phenoxyl radicals. Synthetically, the microcrystalline, paramagnetic (μ_{eff} = 1.7 μ_B), solid material of $[Zn(L^4)(Ph_2acac)]PF_6$ (**5**) was produced by one electron oxidation of **4** by 1 equiv of ferrocenium hexafluorophosphate in dry CH_2Cl_2. Oxidation of coordinated phenol pendent arms in **1**, **2**, and **2a** occurs at significantly higher potentials and is irreversible. Electronic (UV−vis), electron paramagnetic resonance (EPR), and resonance Raman (RR) spectra of the radicals have been studied in solution and allow the description of the electronic structure of these coordinated phenoxyl radical complexes.

Introduction

The occurrence of tyrosyl radicals has been established in a number of metalloproteins[1−4] by spectroscopic methods (electron paramagnetic resonance (EPR), resonance Raman (RR), absorption (UV−vis), and in one instance by X-ray crystallography. Well-characterized examples include the R2 subunit of ribonucleotide reductase with a persistent *uncoordinated* tyrosyl radical in close vicinity to a diferric μ-oxo bridged cluster[5−7] and a tyrosyl derivative *coordinated* to a copper(II) ion in the fungal enzyme galactose oxidase (GO).[8−10] In the latter case the assignment of oxidation state as Cu(II)-tyrosyl *versus* Cu(III)-tyrosinate is based on spectroscopic features of the chromophore: (i) the active form of GO is EPR-silent,[11] probably due to intramolecular antiferromagnetic coupling between the tyrosyl radical and the Cu(II) (d^9) center; (ii)—more directly—the electronic spectrum of the active form resembles features characteristic of phenoxyl radicals, *i.e.*, a strong absorption at 445 nm (ϵ > 5000 M^{-1} cm^{-1}) which is not present in the one-electron reduced form;[12] (iii) the RR spectrum[13,14] of active GO shows features which closely resemble those of genuine phenoxyl radicals, *i.e.*, a ν(C−O•) and a ν(C═C) stretching frequency at 1487 and 1595 cm^{-1}, respectively, and (iv) the X-ray absorption Cu K-edge spectra of the active and one-electron reduced Cu(II) state of GO do not show a shift of the Cu K-edge energy excluding an oxidation state change of Cu(III) → Cu(II).[15]

The crystal structure determination of the inactive form of GO [9,10] has revealed an active site as depicted in Figure 1 where the Cu(II) ion is in square pyramidal environment of an axially and an equatorially bound tyrosine (or tyrosinate), two histidine residues, and an acetate (or water) ligand. The equatorially bound Tyr272 is modified by a covalent C−S bond to Cys228, which lowers the redox potential for radical formation. In the catalytic cycle, intriguing protonation−deprotonation steps have been invoked where bound and uncoordinated tyrosine (phenol) ligands and their coordinated tyrosinate (phenolate) analogs as well as the oxidized, bound tyrosyl form play an interesting role.[16]

[⊗] Abstract published in *Advance ACS Abstracts,* September 1, 1997.

(1) Stubbe, J. A. *Biochemistry* **1988**, *27*, 3893.
(2) Stubbe, J. A. *Annu. Rev. Biochem.* **1989**, *58*, 257.
(3) *Metal Ions in Biological Systems*; Sigel, H., Sigel, A., Eds.; 1994; Vol 30.
(4) Fontecave, M.; Pierre, J.-L. *Bull. Soc. Chim. Fr.* **1996**, *133*, 653.
(5) Ehrenberg, A.; Reichard, P. *J. Biol. Chem.* **1972**, *247*, 3485.
(6) Fontecave, M.; Nordlund, P.; Eklund, H.; Reichard, P. In *Advances in Enzymology and Related Areas of Molecular Biology*; Meister, A., Ed.; John Wiley and Sons: New York, 1992; Vol. 65, pp 147−183.
(7) Stubbe, J. In *Advances in Enzymology and Related Areas of Molecular Biology;* Meister, A., Ed.; John Wiley and Sons: New York, 1990; Vol. 63, pp 349−420.
(8) (a) Whittaker, J. W. In *Metal Ions in Biological Systems*; Sigel, H., Sigel A., Eds.; Marcel Dekker, Inc.: 1994; Vol. 30, pp 315−360. (b) Ettinger, M. J.; Kosman, D. J. In *Copper Proteins*; Spiro, T. G., Ed.; John Wiley and Sons: New York, 1981; pp 220−261.
(9) Ito, N.; Phillips, S. E. V.; Yadav, K. D. S.; Knowles, P. F. *J. Mol. Biol.* **1994**, *238*, 794.
(10) Ito, N.; Phillips, S. E. V.; Stevens, C.; Ogel, Z. B.; McPherson, M. J.; Keen, J. N.; Yadav, K. D. S.; Knowles, P. F. *Nature* **1991**, *350*, 87.
(11) (a) Dyrkacz, G. R.; Libby, R. D.; Hamilton, G. A. *J. Am. Chem. Soc.* **1977**, *99*, 2195. (b) Babcock, G. T.; El-Deeb, M. K.; Sandusky, P. O.; Whittaker, M. M.; Whittaker, J. W. *J. Am. Chem. Soc.* **1992**, *114*, 3727.
(12) Whittaker, M. M.; Whittaker, J. W. *J. Biol. Chem.* **1988**, *263*, 6074.
(13) Whittaker, M. M.; De Vito, V. L.; Asher, S. A.; Whittaker, J. W. *J. Biol. Chem.* **1989**, *264*, 7104.
(14) McGlashen, M. L.; Eads, D. D.; Spiro, T. G.; Whittaker, J. W. *J. Phys. Chem.* **1995**, *99*, 4918.
(15) (a) Clark, K.; Penner-Hahn, J. E.; Whittaker, M. M.; Whittaker, J. W. *J. Am. Chem. Soc.* **1990**, *112*, 6433. (b) Knowles, P. F.; Brown III, R. D.; Koenig, S. H.; Wang, S.; Scott, R. A.; McGuirl, M. A.; Brown, D. E.; Dooley, D. M. *Inorg. Chem.* **1995**, *34*, 3895.

S0002-7863(97)00417-4 CCC: $14.00

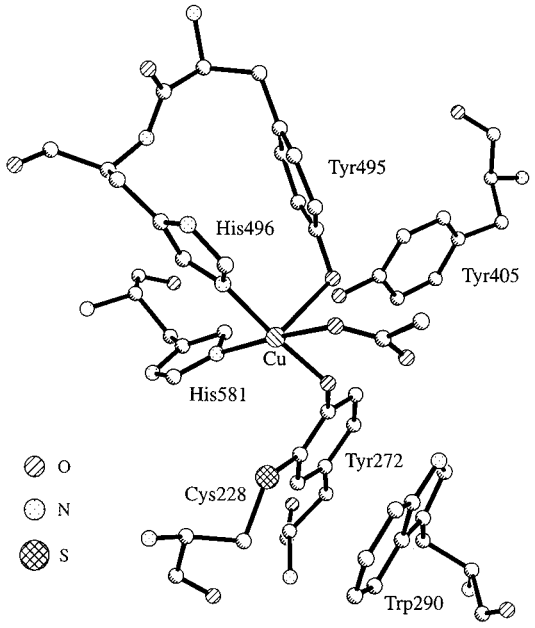

Figure 1. Schematic representation of the active site of the inactive form of Galactose oxidase (pH = 4.5) using atom coordinates from the Brookhaven National Laboratory Protein Data Bank.

While low-molecular weight, crystallographically characterized transition metal complexes with coordinated phenolate ligands including those of copper(II)[17] are well known, their analogs containing coordinated phenol ligands are by far less well understood,[18] and the chemistry of coordinated phenoxyl radicals is still in its infancy.[19] Only very recently, we and others have been able to produce such complexes of Fe,[20,21] Ga,[21] Sc,[21] Cr,[22] and Cu,[23] and only in one instance such a species has been structurally characterized by X-ray crystallography, namely $[Cr^{III}(L^2)](ClO_4)$.[22] Model complexes of this kind are important because they allow to establish definitively the spectroscopic features of *coordinated vs uncoordinated* phenoxyl radicals and to understand their chemical reactivity.

The synthesis of transition metal complexes containing phenoxyl radicals has been hampered by the inherent reactivity of the ligand.[24] Stable phenoxyl radicals are available only when the ortho- and para-positions at the aromatic ring are protected by bulky nonoxidizable groups, *e.g.*, a *tert*-butyl group. Otherwise a variety of side reactions including dimerization (radical coupling) will destroy the radical. Secondly, the transition metal ion-to-phenoxyl bond is thermodynamically less stable[22] than the corresponding bond to a phenolate. This leads to a situation where monodentate phenoxyl ligands will rapidly dissociate.

In order to circumvent both synthetic problems we and others have made use of pendent arm macrocycles with a 1,4,7-triazacyclononane backbone and one, two, or three phenolate pendent arms.[25−29] These tetra-, penta-, and hexadentate ligands bind very strongly to di- and trivalent transition metal ions.[30,31] Here we use the macrocycles L^1H_3, L^2H_3, L^3H, and L^4H shown in Scheme 1.

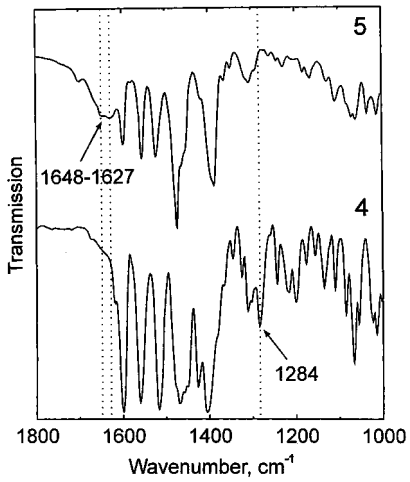

Figure 2. Infrared spectra of **4** and **5** (KBr-disks) in the region 1000−1800 cm^{-1}.

We have synthesized their complexes with zinc(II) for a variety of reasons. Zinc(II) with a d^{10} electronic configuration is redox-innocent in a wide potential range. Thus, all observable redox processes of its complexes must be ligand centered. Secondly, if phenoxyl radical species are generated, they are paramagnetic ($S = 1/2$) and should be ideally suited for EPR spectroscopic characterization. In addition, the electronic spectra of such species are unperturbed by d−d transitions. Therefore, these ligand centered chromophores can be readily investigated by RR spectroscopy. Finally, zinc(II) is a much weaker Lewis acid than the trivalent metal ions Ga(III) and Sc(III). It was hoped that coordinated phenol complexes might also become synthetically accessible which was not the case for $[Ga(L^{1,2})]$ and $[Sc(L^{1,2})]$ complexes.[21]

A zinc complex containing an *uncoordinated* phenoxyl radical, namely $[Zn(BIDPhE)Cl_2]$ (BIDPhE = 1,1-bis[2-(1-methylimidazolyl]-1-(3,5-di-*tert*-butyl-4-oxylphenyl)ethane, has recently been described.[32] Its spectroscopic properties (UV−vis, EPR, and RR) provide a useful basis for the interpretation of our data on complexes containing *coordinated* phenoxyl radicals.

Results

Syntheses. The syntheses of the macrocyclic pendent arm ligands L^1H_3 and L^2H_3 (Scheme 1) have been described previously as have their isotopomers deuterated at the benzylic groups, d_6-L^1H_3 and d_6-L^2H_3.[21] The ligand 1,4-dimethyl-7-(3,5-di-*tert*-butyl-2-hydroxybenzyl)-1,4,7-triazacyclononane (L^3H) has been obtained from the reaction of 1 equiv of 1,4-dimethyl-1,4,7-triazacyclononane with 1 equiv of 2-hydroxy-3,5-di-*tert*-

(16) Wachter, R. M.; Branchaud, B. P. *J. Am. Chem. Soc.* **1996**, *118*, 2782.
(17) Whittaker, M. M.; Chuang, Y.-Y.; Whittaker, J. W. *J. Am. Chem. Soc.* **1993**, *115*, 10029.
(18) Auerbach, U.; Eckert, U.; Wieghardt, K.; Nuber, B.; Weiss, J. *Inorg. Chem.* **1990**, *29*, 938.
(19) Goldberg, D. P.; Lippard, S. J. In *Mechanistic Bioinorganic Chemistry*; Thorp, H. H., Pecoraro, V. L., Eds.; Advances in Chemistry 246; American Chemical Society: Washington, D.C., 1995; p 61.
(20) Hockertz, J.; Steenken, S.; Wieghardt, K.; Hildebrandt, P. *J. Am. Chem. Soc.* **1993**, *115*, 11222.
(21) Adam, B.; Bill, E.; Bothe, E.; Goerdt, B.; Haselhorst, G.; Hildenbrand, K.; Sokolowski, A.; Steenken, S.; Weyhermüller, T.; Wieghardt, K. *Chem. Eur. J.* **1997**, *3*, 308.
(22) Sokolowski, A.; Bothe, E.; Bill, E.; Weyhermüller, T.; Wieghardt, K. *J. Chem. Soc., Chem. Commun.* **1996**, 1671.
(23) (a) Halfen, J. A.; Young, V. G.; Tolman, W. B. *Angew. Chem.* **1996**, *108*, 1832; *Angew. Chem., Int. Ed. Engl.* **1996**, *35*, 1687. (b) Halfen, J. A.; Jazdzewski, B. A.; Mahapatra, S.; Berreau, L. M.; Wilkinson, E. C.; Que, Jr., L.; Tolman, W. B. *J. Am. Chem. Soc.* **1997**, in press.
(24) Altwicker, E. R. *Chem. Rev.* **1967**, *67*, 475.
(25) Moore, D. A.; Fanwick, P. E.; Welch, M. J. *Inorg. Chem.* **1989**, *28*, 1504.
(26) Auerbach, U.; Weyhermüller, T.; Wieghardt, K.; Nuber, B.; Bill, E.; Butzlaff, C.; Trautwein, A. X. *Inorg. Chem.* **1993**, *32*, 508.
(27) Martell, A. E.; Motekaitis, R. J.; Welch, M. J. *J. Chem. Soc., Chem. Commun.* **1990**, 1748.
(28) Flassbeck, C.; Wieghardt, K. *Z. Anorg. Allg. Chem.* **1992**, *608*, 60.
(29) Stockheim, C.; Hoster, L.; Weyhermüller, T.; Wieghardt, K.; Nuber, B. *J. Chem. Soc., Dalton Trans.* **1996**, 4409.
(30) Clarke, E. T.; Martell, A. E. *Inorg. Chim. Acta* **1991**, *186*, 103.
(31) Motekaitis, M. J.; Sun, Y.; Martell, A. E. *Inorg. Chim. Acta* **1992**, *198−200*, 421.
(32) Goldberg, D. P.; Watton, S. P.; Maschelein, A.; Wimmer, L.; Lippard, S. J. *J. Am. Chem. Soc.* **1993**, *115*, 5346.

Scheme 1. Ligands and Complexes

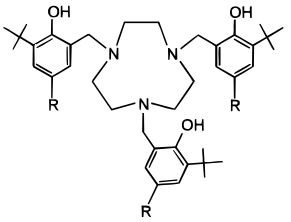

R: *tert*-butyl L^1H_3

methoxy L^2H_3

$[Zn(L^1H_2)]BF_4 \cdot H_2O$ **1**

$[Zn(L^2H_2)]BF_4 \cdot H_2O$ **2**

$[Zn(L^2H)]$ **2a**

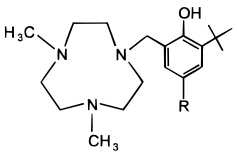

R: *tert*-butyl L^3H

methoxy L^4H

$[Zn(L^3)(Ph_2acac)]$ **3**

$[Zn(L^4)(Ph_2acac)]$ **4**

$[Zn(L^4)(Ph_2acac)]PF_6$ **5**

$[Zn(L^4)(Me\text{-}acac)]$ **6**

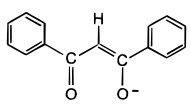

Ph_2acac^-

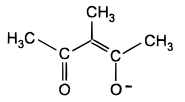

$Me\text{-}acac^-$

butyl-benzylbromide in dry toluene in the presence of KOH. Sodium [1,4-dimethyl-7-(3-*tert*-butyl-5-methoxy-2-hydroxybenzyl)-1,4,7-triazacyclononane], Na[L^4], was obtained from a Mannich reaction of 1,4-dimethyl-1,4,7-triazacyclononane, paraformaldehyde, $(CH_2O)_n$, and 2-*tert*-butyl-4-methoxyphenol in methanol. After exchange of the solvent methanol for dry tetrahydrofuran and addition of 1 equiv of NaH the sodium salt Na[L^4] was obtained as pale-yellow solid. By using $(CD_2O)_n$ and CH_3OD for the above synthesis the compound Na[d_2-L^4] selectively deuterated at the benzylic group was obtained.

The reaction of $Zn(BF_4)_2 \cdot 4H_2O$ in acetonitrile with the macrocyclic pendent arm ligands L^1H_3 and L^2H_3 in the ratio 1:1, respectively, affords colorless precipitates of $[Zn(L^1H_2)]BF_4 \cdot H_2O$ (**1**) and $[Zn(L^2H_2)]BF_4 \cdot H_2O$ (**2**). Treatment of a methanolic solution of **2** with KOH results in the formation of a colorless precipitate of the neutral compound $[Zn(L^2H)]$ (**2a**). From similar reaction mixtures of L^3H and [L^4]Na with $Zn(BF_4)_2 \cdot 4H_2O$ in methanol (1:1) to which 1 equiv of potassium 1,3-diphenyl-1,3-propanedionate (Ph_2acac) or, alternatively, 3-methyl-2,4-pentanedionate (Me-acac) has been added, yellow, microcrystalline precipitates of $[Zn(L^3)(Ph_2acac)]$ (**3**), $[Zn(L^4)(Ph_2acac)]$ (**4**), and $[Zn(L^4)(Me\text{-}acac)]$ (**6**) formed, respectively.

It is possible to oxidize complex **4** by one electron with 1 equiv of ferrocenium hexafluorophosphate in dry CH_2Cl_2 solution. From the solution a green-brown microcrystalline precipitate of $[Zn(L^4)(Ph_2acac)]PF_6$ (**5**) was obtained in 24% yield. Measurement of the temperature-dependent magnetic susceptibility (100−300 K) of a powdered sample revealed that **5** is paramagnetic with an effective magnetic moment, μ_{eff} (298 K), of 1.7 μ_B. Complex **5** is quite stable in the solid state and in solution, but it is easily reduced by an appropriate reducing agent to the colorless neutral species **4**.

Figure 2 shows a comparison of the infrared spectra of **4** and **5** in the range 1800−1000 cm^{-1}. Two features are remarkable. The ν(C−O) stretching frequency of the coordinated phenolate in **4** is observed at 1284 cm^{-1} but is *absent* in **5**. On the other hand, **4** does not show bands >1605 cm^{-1}, but in the spectrum of the oxidized form, **5**, new features appear in this region

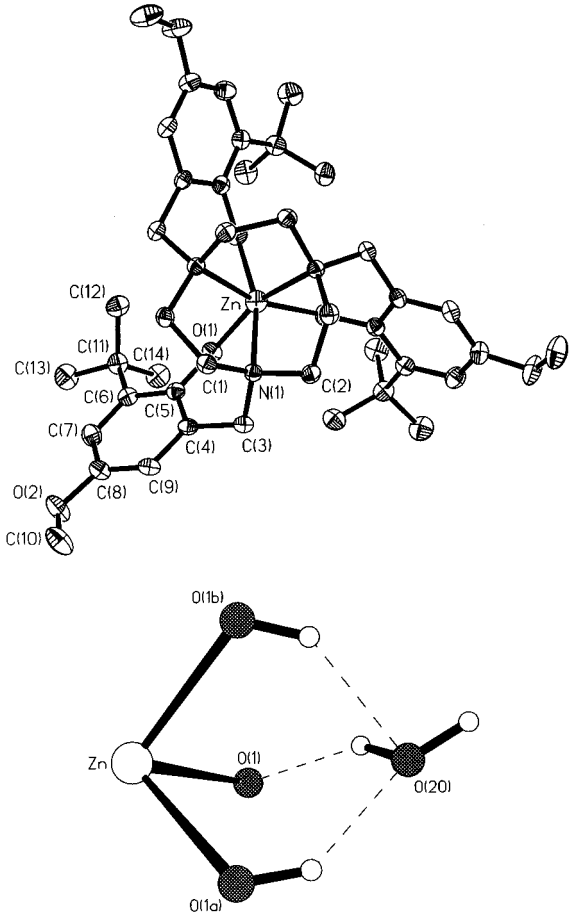

Figure 3. (a) Average structure of the cation in crystals of **2** (without hydrogen atoms). (b) Possible hydrogen bonding scheme between the cation and a water molecule of crystallization. Note that atoms Zn and O(20) lie on a 3-fold crystallographic axis. Small open circles represent hydrogen atoms.

(1627−1648 cm^{-1}). These bands are assigned to ν(C═C) stretching frequencies (see below) in accordance with a quinone-like resonance structure of coordinated phenoxyls. The ν(C−O•) stretching frequency expected for phenoxyl radicals at ∼1500 cm^{-1} has not been unambiguously identified in the spectrum of **5** due to ν(C═O) bands of the coordinated Ph_2acac^- ligand in both **4** and **5**.

The ^{1}H NMR spectra of **3**, **4**, and **6** in $CDCl_3$ solution at 20 °C show unambiguously that a stable conformation of the six-membered chelate ring, Zn−O−C−C−C−N, of the coordinated phenolate pendent arm is retained in solution since the protons of the benzyl group are diastereotopic.

In contrast, in the corresponding spectra of **1** and **2** in CD_3CN solution at 20 °C only a singlet is observed for the six benzylic protons; these protons are magnetically equivalent on the time scale of a ^{1}H NMR experiment (∼10^{-4} s). This implies that under these experimental conditions the phenol pendent arms undergo rapid deprotonation−protonation. In the spectrum of **2a** in CD_2Cl_2 at ambient temperature the six benzylic protons are again diastereotopic giving rise to two doublets at $\delta = 2.97$ and 4.24 ($J = 10.78$ Hz). This indicates that the two phenolates and the phenol pendent arm are coordinated but equivalent due to a rapid deprotonation−protonation equilibrium. The spectrum of $[Zn(L^2)]^-$ in CD_2Cl_2 solution also shows two doublets for six benzylic protons.

Crystal Structures. The structures of **2**, **3**·0.5 toluene·1n-hexane, and **4** have been determined by single-crystal X-ray crystallography at 173(2) (**2**) and 100(2)K (**3**, **4**). Figures 3−5 show the structures of the monocation $[Zn(L^1H_2)]^+$ in **2** and of

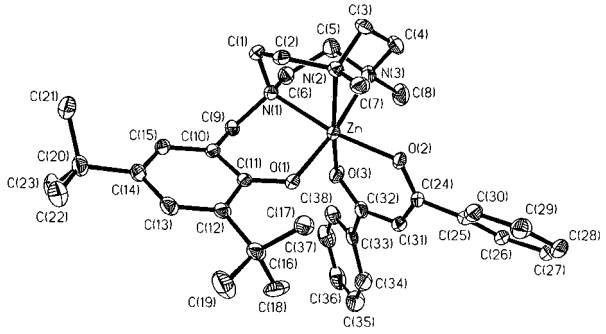

Figure 4. Structure of the neutral complex in crystals of **3**·0.5toluene·-1n-hexane.

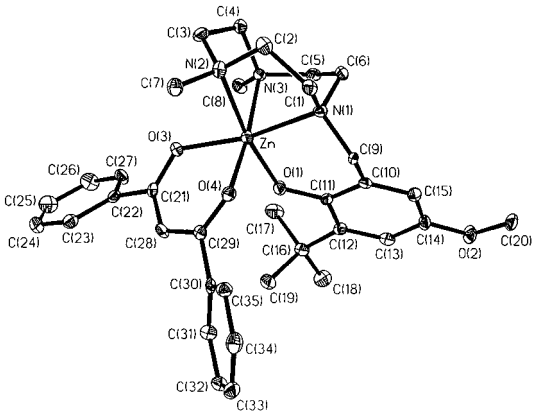

Figure 5. Structure of the neutral complex in crystals of **4**.

the neutral complexes in crystals of **3** and **4**, respectively. Table 1 summarizes selected bond distances and angles.

The monocation in **2** possesses crystallographically imposed C_3 symmetry which is not compatible with the fact that it contains two coordinated phenolic and one bound phenolate pendent arm of the monoanionic macrocycle $[L^1H_2]^-$. As a consequence, a static disorder is observed which has been successfully modeled. One water molecule of crystallization is in close vicinity to the three facial oxygen donor atoms of the cation via hydrogen bonding contacts (O1···O(20) 2.661-(4) Å). The oxygen atom O(20) of this H_2O molecule lies on a crystallographic C_3 axis. In the difference Fourier map two residual electron density maxima per asymmetric unit were located within bonding distance to this oxygen. In addition, a further hydrogen atom was located in close proximity to the coordinated phenol/phenolate oxygen O(1). These positions were satisfactorily refined without restraints by using the occupancy factor 0.33 for each hydrogen atom of H_2O and 0.66 for those bound to the phenol oxygen. Figure 3b shows that this can be interpreted as a 3-fold superposition where two coordinated phenol groups form hydrogen bonds to the oxygen atom of the water molecule ($O_{phenol}-H\cdots O_{water}$) and one hydrogen bonding contact is of the type $O_{phenolate}\cdots H-O_{water}$. Due to this disorder it is not possible to distinguish the bonding distances between a zinc-to-phenol and that of zinc-to-phenolate bond, but the average distance of 2.173(2) Å is significantly longer than genuine zinc−phenolate bonds in **3** and **4** at 1.981-(2) and 1.962(2) Å. This is in agreement with the fact that phenolates are better ligands than phenols.

In all structures the zinc ion is six coordinate in a distorted octahedral environment of the three facially bound amine nitrogen donors and three oxygen donors which are phenol, phenolate, or 1,3-diphenyl-1,3-propanedionate derived.

Interestingly, in structures **3** and **4** the phenolate is very strongly bound ($Zn-O_{phen}$ = 1.981(2) in **3** and 1.962(3) Å in **4**) and exerts a significant trans-influence on the Zn−N bond in trans-position.

Table 1. Selected Bond Distances (Å) and Angles (deg) of **2**, **3**·0.5Toluene·1n-Hexane, and **4**

Complex **2**			
Zn−N1	2.160(2)	N1−C3	1.492(3)
Zn−O1	2.173(2)	N1−C1	1.495(3)
O1−C5	1.384(3)	O2−C10	1.419(4)
O1−H	0.85(3)	C1−C2	1.530(3)
O2−C8	1.375(4)	C3−C4	1.505(4)
N1−Zn−N1′	82.64(8)	Zn−O1−H	115(3)
N1−Zn−O1	85.95(7)	C5−O1−H	118(3)
N1−Zn−O1′	164.60(7)	Zn−O1−C5	127.0(2)
N1−Zn−O1″	106.15(7)		
Complex **3**·0.5Toluene·1n-Hexane			
Zn−O1	1.981(2)	Zn−O2	2.038(2)
Zn−O3	2.091(2)	Zn−N1	2.177(2)
Zn−N2	2.249(2)	Zn−N3	2.279(2)
O1−C11	1.312(3)		
O2−C24	1.273(3)		
O3−C32	1.260(3)		
O1−Zn−O2	95.08(7)	O1−Zn−O3	92.00(8)
O2−Zn−O3	89.35(7)	O1−Zn−N1	92.08(7)
O2−Zn−N1	170.86(7)	O3−Zn−N1	96.09(8)
O1−Zn−N2	100.56(8)	O2−Zn−N2	93.14(7)
O3−Zn−N2	166.91(8)	N1−Zn−N2	79.93(8)
O1−Zn−N3	172.14(8)	O2−Zn−N3	92.78(8)
O3−Zn−N3	88.28(8)	N1−Zn−N3	80.08(8)
N2−Zn−N3	78.77(9)	C11−O1−Zn	129.2(2)
C24−O2−Zn	124.9(2)	C32−O3−Zn	123.9(2)
Complex **4**			
Zn−O1	1.962(3)	Zn−O3	2.069(3)
Zn−O4	2.124(3)	Zn−N1	2.172(3)
Zn−N3	2.210(3)	Zn−N2	2.265(4)
O1−C11	1.322(5)	O2−C14	1.384(5)
O2−C20	1.432(5)	O3−C21	1.269(5)
O4−C29	1.271(5)		
O1−Zn−O3	96.8(1)	O1−Zn−O4	91.9(1)
O3−Zn−O4	87.5(1)	O1−Zn−N1	91.9(1)
O3−Zn−N1	170.2(1)	O4−Zn−N1	96.9(1)
O1−Zn−N3	97.4(1)	O3−Zn−N3	92.1(1)
O4−Zn−N3	170.6(1)	N1−Zn−N3	82.1(1)
O1−Zn−N2	171.3(1)	O3−Zn−N2	91.5(1)
O4−Zn−N2	91.1(1)	N1−Zn−N2	79.7(1)
N3−Zn−N2	79.5(1)	C11−O1−Zn	130.6(3)
C29−O4−Zn	119.3(3)	C21−O3−Zn	123.6(3)

Table 2. Redox Potentials of Complexes[a] *vs* Fc^+/Fc

complex	solvent	$E_{1/2}$, V			E_p^{ox}, V
1	CH_3CN	0.39 (rev)			+1.40 (irr)
2	CH_3CN	0.17 (rev)			+0.94 (irr)
2a	CH_2Cl_2	−0.28 (rev)	−0.05 (rev)		+0.80 (irr)
$[Zn(L^2)]^-$ [b]	CH_2Cl_2	−0.63 (rev)	−0.28 (rev)	−0.06 (rev)	
3	CH_2Cl_2	−0.09 (rev)			
4	CH_2Cl_2	−0.28 (rev)			
5	CH_2Cl_2	−0.28 (rev)			
6	CH_2Cl_2	−0.32 (rev)			

[a] Conditions: 0.10 M $[N(n\text{-but})_4]PF_6$ supporting electrolyte; glassy-carbon working electrode; T = 298 K; reference electrode: Ag/AgCl ($LiCl/C_2H_5OH$) or $Ag/AgNO_3$. Cvs were recorded at scan rates 20−500 mV s^{-1}; square-wave voltammograms were recorded at 30 Hz frequency and 25 mV pulse height. [b] This species was generated from **2a** by addition of 1 equiv of $K[OC(CH_3)_3]$.

Electrochemistry. The electrochemistry of complexes has been investigated by cyclic and square-wave voltammetry as well as coulometry in CH_2Cl_2 or CH_3CN solution containing 0.10 M $[N(n\text{-but})_4]PF_6$ as supporting electrolyte. All potentials are referenced *vs* the ferrocenium/ferrocene (Fc^+/Fc) couple; the results are summarized in Table 2.

For the sake of clarity we will first discuss the cyclic voltammograms (cv) of **3**, **4**, and **6**. The insets of Figure 6 show the cvs of **3**, **4**, and **6**. In the potential range +0.5 to −2.0 V the three species display a single reversible one-electron transfer wave. Coulometry at a constant potential of +0.10 V and ambient temperature established that **3**, **4**, and **6** undergo a

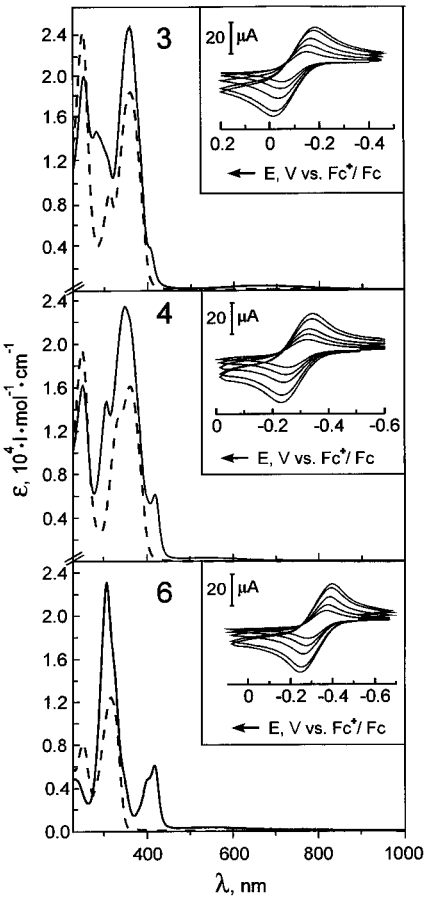

Figure 6. Electronic absorption spectra of complexes **3** (top), **4** (middle), and **6** (bottom) in CH_2Cl_2 (dashed lines) and their electrochemically generated one-electron oxidized forms (full lines) $[\mathbf{3}]^{\bullet+}$, $[\mathbf{4}]^{\bullet+}$, and $[\mathbf{6}]^{\bullet+}$, respectively. The insets show the respective cyclic voltammograms recorded at scan rates 500, 400, 200, 100, and 50 mV s^{-1} in CH_2Cl_2 (0.10 M $[N(n\text{-but})_4]PF_6$).

one-electron oxidation, eq 1, respectively. During this oxidation

$$\mathbf{3}\ (\mathbf{4},\ \mathbf{6}) \rightleftharpoons [\mathbf{3}]^{\bullet+}\ ([\mathbf{4}]^{\bullet+},\ [\mathbf{6}]^{\bullet+}) + e \qquad (1)$$

the color of the solution changed from yellow to green. A cv of such green CH_2Cl_2 solution showed that no decomposition of the oxidized species had occurred during the coulometry experiment. Thus, solutions of $[\mathbf{3}]^{\bullet+}$, $[\mathbf{4}]^{\bullet+}$, and $[\mathbf{6}]^{\bullet+}$ are stable at room temperature. Complex **3** is more difficult to oxidize than **4** by 0.19 V.

Interestingly, the cvs of **1** and **2** in CH_3CN (Figure 7a) which each contain two coordinated phenols and one phenolate pendent arm also display only one reversible one-electron transfer wave at 0.39 and 0.17 V, respectively. We assign this process to the reversible formation of one coordinated phenoxyl radical as in eqs 2 and 3. The potential difference of 220 mV for **1** and **2** which is nearly the same as between **3** and **4** reflects the differing oxidizability of *tert*-butyl and methoxy substituted phenolates in $[L^1H_2]^-$ and $[L^2H_2]^-$, respectively. At potentials >0.9 V the cv reveals an irreversible oxidation which is probably due to the irreversible oxidation of the coordinated phenol groups.

$$[Zn(L^1H_2)]^+ \rightleftharpoons [Zn(L^1H_2)]^{\bullet 2+} + e \qquad (2)$$

$$\underset{\text{colorless}}{[Zn(L^2H_2)]^+} \rightleftharpoons \underset{\text{yellow-green}}{[Zn(L^2H_2)]^{\bullet 2+}} + e \qquad (3)$$

Considering the fact that in complexes **1** and **3** (or **2** and **4**) the same Zn−O−R unit is oxidized, it is at first sight surprising

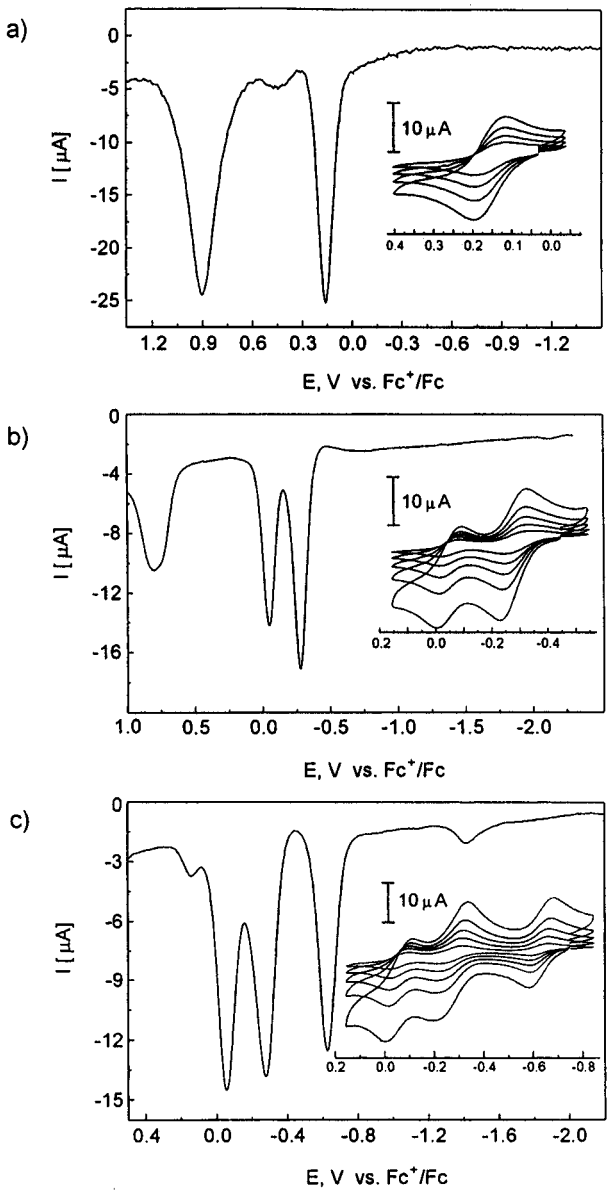

Figure 7. (a) Square-wave (30 Hz, pulse height 25 mV) and cyclic (inset) voltammograms of **2** in CH_3CN (0.10 M $[N(n\text{-but})_4]PF_6$) at 298 K at a glassy carbon working electrode (scan rates: 200, 100, 50, and 20 mV s^{-1}). (b) Square-wave and cyclic (inset) voltammogram of **2a** in CH_3CN (0.10 M $[N(n\text{-but})_4]PF_6$) at 298 K (scan rates: 500, 200, 100, 50, 20 mV s^{-1}). Other experimental conditions are as above. (c) Square-wave and cyclic (inset) voltammogram of **2a** in CH_2Cl_2 (0.10 M $[N(n\text{-but})_4]PF_6$) to which 1 equiv of K $[OC(CH_3)_3]$ has been added (scan rates as in b)). Other experimental conditions are as above.

that **3** is easier to oxidize than **1** (or **4** than **2**) by 480 mV (or 450 mV). We interpret this as a purely electrostatic effect since oxidation of the monocation in **1** yields a dication, whereas the neutral species **3** is oxidized to afford a monocation. Differences in the respective solvation energies may account for the potential differences. This has previously been shown to be the case for neutral $[Ga(L^1)]$ and $[Ga(L^2)]$, where the three identical coordinated phenolate pendent arms are successively oxidized to give the respective mono-, di-, and trication.[21] The redox potentials $E^1_{1/2}$, $E^2_{1/2}$, and $E^3_{1/2}$ for these one-electron transfer processes differ by 200−270 mV per electron transfer step.

The cv of the neutral species **2a** dissolved in CH_2Cl_2 is shown in Figure 7b. Clearly, *two* reversible one-electron transfer processes are observed at −0.28 and −0.05 V which are assigned to the successive oxidation of two coordinated phenolate pendent arms. The coordinated phenol is irreversibly oxidized at $E_p$ox = +0.80 V. Thus, generation of the first

Scheme 2. Electrochemically Identified Equilibria of **2** (and **2a**)[a]

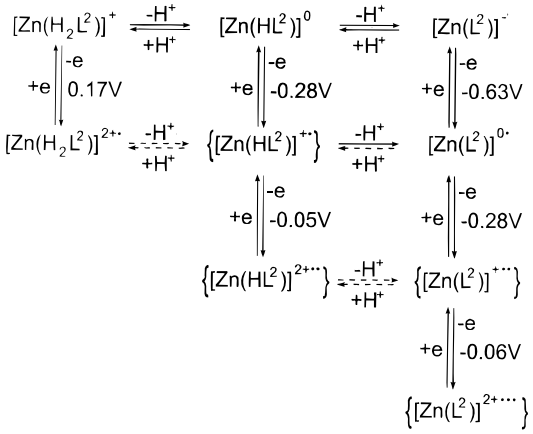

[a] The potentials refer to experiments in CH_2Cl_2 (0.1 M [TBA]PF_6) and are referenced *vs* the Fc^+/Fc couple. Dotted arrows indicate equilibria which have not been established experimentally; species in { } have only been generated by cyclic voltammetry; they are not stable in solution at 20 °C.

coordinated phenoxyl radical in **2a** is easier by 450 mV than in **2** which again reflects the difference in solvation energies for the two processes.

We have also generated the monoanionic form of **2**, $[Zn(L^2)]^-$, in CH_2Cl_2 solution from **2a** by addition of 1 equiv of potassium *tert*-butyloxide and recorded its cv (Figure 7c). This monoanion contains three coordinated phenolate pendent arms, and, consequently, *three* reversible one-electron transfer waves are observed at $E_{1/2} = -0.63$, -0.28, and -0.05 V which were assigned to the formation of the mono-, bis-, and trisphenoxyl radical complexes as in eq 4, respectively. Scheme 2 summarizes the species generated from **2**, **2a** via protonation−deprotonation and one-electron oxidation reactions.

$$[Zn(L^2)]^- \underset{+e}{\overset{-e}{\rightleftharpoons}} [Zn(L^2)]^{\bullet} \underset{+e}{\overset{-e}{\rightleftharpoons}} [Zn(L^2)]^{\bullet\bullet+} \underset{+e}{\overset{-e}{\rightleftharpoons}} [Zn(L^2)]^{\bullet\bullet\bullet 2+} \quad (4)$$

EPR Spectroscopy. X-band EPR spectroscopy on CH_3CN or CH_2Cl_2 solutions at 298 K of the electrochemically one-electron oxidized forms of **1**, **2**, **3**, **4**, **6** and of $[Zn(L^2)]^-$ proved to be informative because they all contain one coordinated phenoxyl radical ($S = 1/2$) ligand. At 298 K the six radical species display signals at $g_{iso} = 2.0045 \pm 0.0002$ which is characteristic for phenoxyl radicals.[24] Table 3 summarizes the results.

Figure 8 displays the EPR spectra of $[\mathbf{3}]^{\bullet+}$ and $[d_2\text{-}\mathbf{3}]^{\bullet+}$. The spectra were satisfactorily simulated by taking into account hyperfine coupling with *one* benzylic proton only. Hyperfine coupling to the other benzylic proton, to the amine nitrogen, to the two aromatic protons in meta-position, or to the ^{67}Zn ($I = 5/2$) isotope (4.1% natural abundance) was not resolved. The fact that coupling to only one benzylic proton is observed is in line with the RR data (see below) which suggest that the phenoxyl radical is coordinated to the Zn ion. In this case, magnetically inequivalent benzylic protons are expected to be present, as is observed in the ^1H NMR spectrum of diamagnetic **3**.

Identical spectra consisting of eight signals were obtained for $[\mathbf{4}]^{\bullet+}$ and $[\mathbf{6}]^{\bullet+}$ (Figure 9a). They were analyzed in terms of a quartet due to the three methoxy protons ($a_H = 0.200$ mT) which is split into a doublet ($a_H = 0.616$ mT) of doublets ($a_H = 0.139$ mT). Changes in the spectrum induced by selective deuteration of the benzylic position prove that the larger doublet

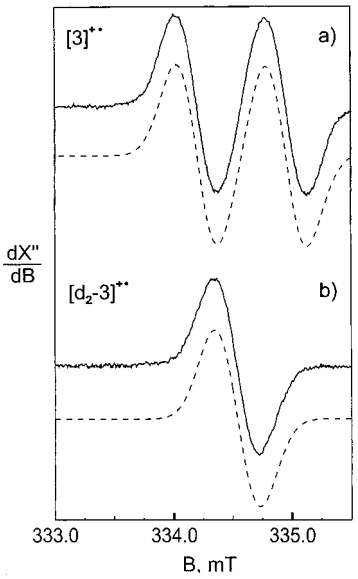

Figure 8. X-band EPR spectrum of electrochemically generated $[\mathbf{3}]^{\bullet+}$ (top) and $[d_2\text{-}\mathbf{3}]^{\bullet+}$ (bottom) in CH_2Cl_2 (0.10 M $[N(n\text{-but})_4]PF_6$) at 298 K (microwave power 0.8 mW; modulation amplitude 0.06 mT, a decrease to 0.002 mT did not allow to resolve any hyperfine splitting). Solid lines are experimental spectra; broken lines represent simulations.

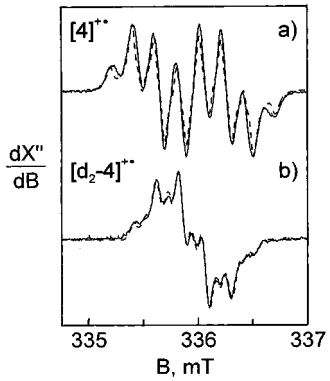

Figure 9. X-band EPR spectra of electrochemically generated $[\mathbf{4}]^{\bullet+}$ (a) and $[d_2\text{-}\mathbf{4}]^{\bullet+}$ (b) in CH_2Cl_2 at 298 K (microwave power 0.4 mW, modulation amplitude 0.06 mT; decreasing the modulation amplitude to 0.002 mT did not improve the resolution). Solid lines: experimental spectra; broken lines: simulations).

arises from hyperfine coupling with this position (Figure 9b). The smaller doublet did not collapse upon deuteration. From a comparison with the identical spectrum of $[\mathbf{6}]^{\bullet+}$ it is obvious that this is not due to coupling to the methine proton of the acac ligand, and, therefore, we assign it to one of the aromatic protons of the coordinated phenoxyl radical. Simulation of the spectrum of $[d_2\text{-}\mathbf{4}]^{\bullet+}$ shows that a further small proton coupling ($a_H = 0.034$ mT, probably due to the other aromatic ring proton) and a nitrogen coupling ($a_N = 0.053$ mT) have to be taken into account.

The EPR spectra of $[Zn(L^1H_2)]^{\bullet 2+}$ and of its benzyl deuterated form $[Zn(d_6\text{-}L^1H_2)]^{\bullet 2+}$ are very similar (Table 2) to those of $[\mathbf{3}]^{\bullet+}$ and $[d_2\text{-}\mathbf{3}]^{\bullet+}$, respectively. Hyperfine coupling to only *one* benzylic proton is detected which suggests that the phenoxyl pendent arm is coordinated to zinc(II) and that the spin is delocalized over one aromatic ring only. The two coordinated phenol groups do not carry significant spin density.

The corresponding spectra of $[Zn(L^2H_2)]^{\bullet 2+}$ and $[Zn(d_6\text{-}L^2H_2)]^{\bullet 2+}$ are shown in Figure 10. From the simulations hyperfine coupling to three methyl protons of one methoxy group, to two aromatic protons in meta position, to *both* magnetically inequivalent benzyl protons, and to one nitrogen

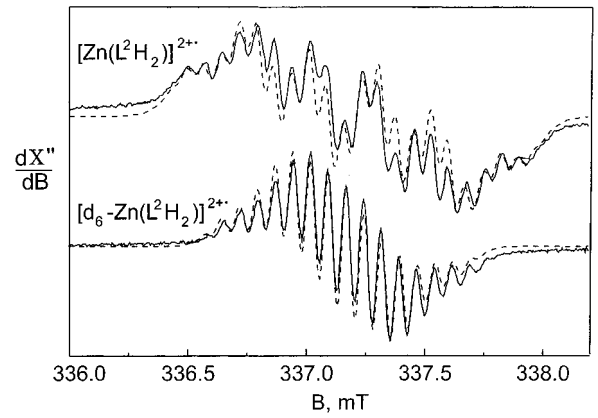

Figure 10. X-band EPR spectra of $[Zn(L^2H_2)]^{\bullet 2+}$ (top) and $[Zn(d_6\text{-}L^2H_2)]^{\bullet 2+}$ in CH_3CN (0.10 M $[N(n\text{-but})_4]PF_6$) at 298 K (microwave power 0.5 mW; modulation amplitude 0.016 mT). Solid lines are experimental spectra; broken lines represent simulations.

Scheme 3. Hyperfine Coupling Constants in mT of $[Zn(L^2H_2)]^{\bullet 2+}$ **[2]**$^{\bullet 2+}$, $[Zn(d_6\text{-}L^2H_2)]^{\bullet 2+}$ $[d_6\text{-}\mathbf{2}]^{\bullet 2+}$, and of **[4]**$^{\bullet +}$ $[d_2\text{-}\mathbf{4}]^{\bullet +}$.

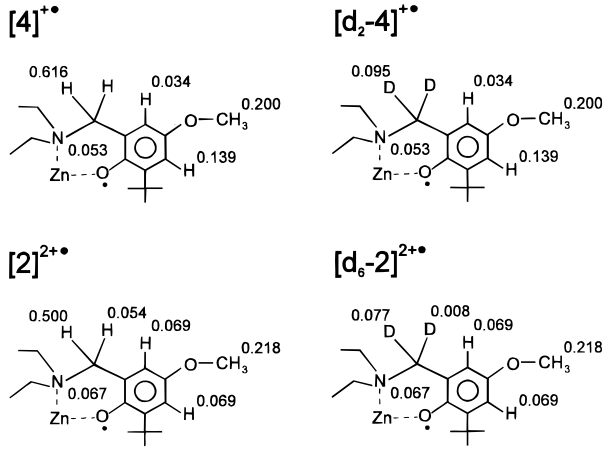

is detected. The values of these coupling constants are close to those observed for **[4]**$^{\bullet +}$. The assignments are shown in Scheme 3.

Like in the case of **[4]**$^{\bullet +}$ the spin of the coordinated phenoxyl radical is localized on one ring. Treatment of a CH_2Cl_2 solution of $[Zn(L^2H_2)]$ with potassium *tert*-butylate yields $[Zn(L^2)]^{\bullet}$ and results in a feature consisting of the multiline spectrum shown in Figure 10 superimposed on a broad unresolved signal. This result is in line with RR data showing the coexistence of protonated and deprotonated species. The broad background signal reminds of the spectra reported for the radicals $[Ga(L^1)]^{\bullet +}$ and $[Sc(L^1)]^{\bullet +}$ which are isostructural with $[Zn(L^2)]^{\bullet}$.[21] Since we had shown previously that the spin in $[Ga(L^1)]^{\bullet +}$ and $[Sc(L^1)]^{\bullet +}$ is delocalized over all three aromatic rings, we suggest that a similar spin distribution prevails in $[Zn(L^2)]^{\bullet}$.

The EPR spectra of radical complexes **[2]**$^{\bullet 2+}$ and **[4]**$^{\bullet +}$ display strong hyperfine coupling to one benzylic proton at $a_H = 0.500$ and 0.616 mT, respectively. Since the phenoxyl radical in both complexes is the same, it is tempting to ascribe the numerical difference between these hyperfine coupling constants, a_H, to small structural differences of the *coordinated* radicals in **[2]**$^{\bullet 2+}$ and **[4]**$^{\bullet +}$. Since the crystal structures of the reduced forms **[2]** and **[4]** have been determined, it is possible to calculate the dihedral angle Θ_1 defined in Scheme 4 of the benzyl protons of the coordinated benzyl phenolates as 36.5° for **[2]** and 26.5° for **[4]**. The ratio of the two $\cos^2\Theta_1$ values is 0.807. If one accepts the following two assumptions that (i) the dihedral angles do not change upon one-electron oxidation (*i.e.*, the radicals remain Zn-bound) and (ii) a McConnell-type, angle-dependent relationship for the hyperfine coupling to the benzylic proton exists where the magnitude of a_H depends on $\cos^2\Theta_1$, then the ratio of a_H for **[2]**$^{\bullet 2+}$ and **[4]**$^{\bullet +}$ should be very similar to that of the $\cos^2\Theta_1$ values. Experimentally, the ratio of the coupling constants is 0.812, in good agreement with the above assumptions. We take this as further corroboration that the phenoxyl radicals are coordinated in both complexes.

Scheme 4. A Model for the Phenoxyl Radicals in **[2]**$^{\bullet 2+}$ and **[4]**$^{\bullet +}$[a]

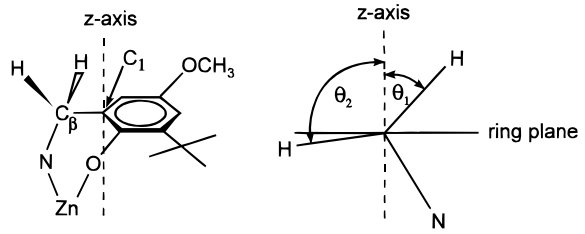

[a] Left: side view; right hand side: end view, looking along the $C_\beta - C_1$ bond of the phenoxyl. The dihedral angle for the more strongly coupled proton, Θ_1, is ~36.5° for **[2]**$^{\bullet 2+}$ and ~26.5° for **[4]**$^{\bullet +}$.

Table 3. EPR Simulation Parameters

complex	solvent	a_H,[a] mT	a_N,[a] mT	a_D,[a] mT	$\Delta\nu$,[b] mT
$[Zn(L^1H_2)]^{\bullet 2+}$ **[1]**$^{\bullet 2+}$	CH_3CN	0.586 (1H)			0.24
$[Zn(d_6\text{-}L^1H_2)]^{\bullet 2+}$	CH_3CN			0.09(1D)	0.22
$[Zn(L^2H_2)]^{\bullet 2+}$ **[2]**$^{\bullet 2+}$	CH_3CN	0.500(1H) 0.054(1H) 0.069(2H) 0.218(3H)	0.067(1N)		0.062
$[Zn(d_6\text{-}L^2H_2)]^{\bullet 2+}$	CH_3CN	0.069(2H) 0.218(3H)	0.067(1N)	0.077(1D) 0.008(1D)	0.045
[3]$^{\bullet +}$	CH_2Cl_2	0.709(1H)			0.200
$[d_2\text{-}\mathbf{3}]^{\bullet +}$	CH_2Cl_2			0.109(1D)	0.187
[4]$^{\bullet +}$	CH_2Cl_2	0.200(3H) 0.616(1H) 0.139(1H) 0.034(1H)	0.053(1N)		0.05
$[d_2\text{-}\mathbf{4}]^{\bullet +}$	CH_2Cl_2	0.200(3H) 0.139(1H) 0.034(1H)	0.053(1N)	0.095(1D)	0.04
[6]$^{\bullet +}$ [c]	CH_2Cl_2				

[a] Hyperfine coupling constant. [b] Line width. [c] The spectrum and simulation parameters of **[6]**$^{\bullet +}$ are identical to those given above for **[4]**$^{\bullet +}$.

Electronic Spectra. Two-phase oxidation of colorless tris-2,4,6-*tert*-butylphenol[34] or 2,4-di-*tert*-butyl-4-methoxyphenol dissolved in CCl_4 with an alkaline aqueous solution of $[Fe(CN)_6]^{3-}$ yields the corresponding persistent yellow phenoxyl radical in the CCl_4 phase. The electronic spectra of these radicals characteristically display a fairly weak absorption maximum at 500−800 nm ($\epsilon \sim 200-500$ L mol^{-1} cm^{-1}) and two intense maxima at 380−440 nm ($\epsilon > 10^3$).[34] These features have finger-print character; they have been identified in proteins such as ribonucleotide reductase[35] and its model complex[33] where the tyrosyl radicals are not bound to a metal ion and in the active form of galactose oxidase.[12]

The electronic spectra of electrochemically generated zinc-bound phenoxyl radicals have been recorded and are summarized in Table 4. For the sake of clarity and simplicity we will first discuss the spectra of colorless **1** and **2** and of their

(33) Goldberg, D. P.; Koulougliotis, D.; Brudvig, G. W.; Lippard, S. J. *J. Am. Chem. Soc.* **1995**, *117*, 3134.
(34) (a) Land, E. J.; Porter, G. *Trans. Faraday Soc. (London)* **1961**, *57*, 1885. (b) Land, E. J.; Porter, G. *Trans. Faraday Soc. (London)* **1963**, *59*, 2016.
(35) (a) Mann, G. J.; Gräslund, A.; Ochiai, E.-I.; Ingemarson, R.; Thelander, L. *Biochemistry* **1991**, *30*, 1939. (b) Sjöberg, B.-M.; Gräslund, A. *Adv. Inorg. Biochem.* **1983**, *5*, 87.

Table 4. Electronic Spectra of Complexes

complex	solvent	λ_{max}, nm (ϵ, L mol^{-1} cm^{-1})
1	CH_3CN	222 (1.6×10^4), 248 sh (3.4×10^3), 280 (4.7×10^3), 300 sh (1.1×10^3)
2	CH_3CN	231 (1.6×10^4), 248 sh (8.1×10^3), 294 (8.3×10^3), 316 sh (3.7×10^3)
2a	CH_2Cl_2	252 (1.8×10^4), 320 (1.0×10^4)
3	CH_2Cl_2	251 (2.4×10^4), 314 (9.2×10^3), 362 (1.85×10^4)
4	CH_2Cl_2	251 (1.9×10^4), 337 sh (1.3×10^4), 362 (1.6×10^4)
6	CH_2Cl_2	252 (8.1×10^3), 316 (1.2×10^4)
$[Zn(L^1H_2)]^{\bullet 2+}$ [a]	CH_3CN	228 (2.1×10^4), 284 (1.6×10^4), 298 (1.2×10^4), 394 sh (3.2×10^3), 408 (3.5×10^3), 700 (320)
$[Zn(L^2H_2)]^{\bullet 2+}$ [a]	CH_3CN	228 sh (1.3×10^4), 303 (1.6×10^4), 334 sh (9.5×10^3), 408 sh (6.9×10^3), 425 (8.3×10^3), 561 (370)
$[Zn(L^2)]^{-}$ [a]	CH_2Cl_2	255 (1.4×10^3), 322 (8.4×10^3)
$[Zn(L^2)]^{\bullet}$ [a]	CH_2Cl_2	248 (7.6×10^3), 306 (1.5×10^4), 338 sh, 402 sh, 419 (6.0×10^3), 522 (350)
$[\mathbf{3}]^{\bullet +}$ [a]	CH_2Cl_2	254 (2.0×10^4), 283 (1.5×10^4), 361 (2.5×10^4), 408 (3.8×10^3), 672 (320)
$[\mathbf{4}]^{\bullet +}$ [a]	CH_2Cl_2	252 (1.6×10^4), 307 (1.5×10^4), 350 (2.3×10^4), 419 (6.1×10^3), 543 (310)
$[\mathbf{6}]^{\bullet +}$ [a]	CH_2Cl_2	305 (2.3×10^4), 401 sh (4.8×10^3), 418 (6.0×10^3), 545 (280)

[a] Species generated by controlled potential electrolysis in the indicated solvent containing 0.10 M $[N(n\text{-}but)_4]PF_6$.

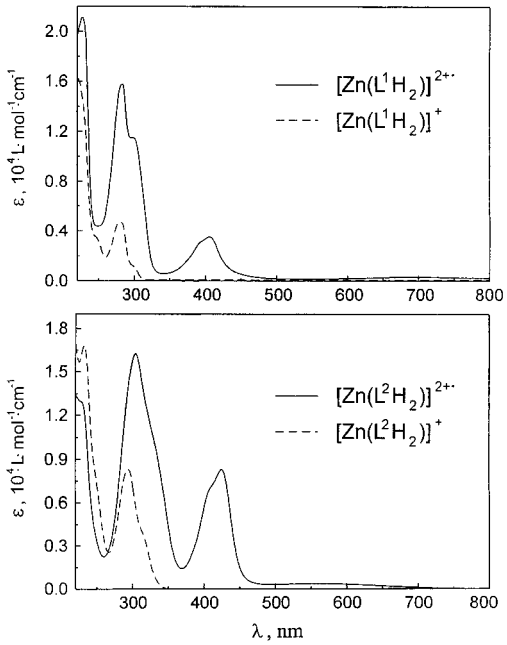

Figure 11. Electronic spectra of **1** and **2** and their one-electron oxidized radicals in CH_3CN at 298 K.

one-electron oxidized, yellow-green radicals $[Zn(L^1H_2)]^{\bullet 2+}$ and $[Zn(L^2H_2)]^{\bullet 2+}$ which are shown in Figure 11. The spectral changes observed upon oxidation of the colorless monocations of **1** and **2** to dications are dramatic and clearly indicate the formation of phenoxyl radicals. The one-electron oxidation of $[Zn(L^2)]^-$ yielding the neutral radical $[Zn(L^2)]^{\bullet}$ is accompanied by similar spectral changes. A comparison of the spectra of $[Zn(L^2H_2)]^{\bullet 2+}$ and $[Zn(L^2)]^{\bullet}$ shows that protonation of the latter shifts the two intense maxima at ~410 nm bathochromically and increases their intensities (Table 4). Complexes **3**, **4**, and **6** have two chromophores, namely the phenolate pendent arm and the 1,3-diphenyl-1,3-propanedionate or 3-methyl-2,4-pentanedionate anion, which display very intense $\pi \rightarrow \pi^*$ transitions at <400 nm. Upon one-electron oxidation new maxima at ~415 nm and ~600 nm again indicate the formation of phenoxyl radicals (see Figure 6).

The electronic spectra of the above coordinated phenoxyl complexes do not differ much from that reported for [Zn(BIDPhE)Cl_2] which contains an uncoordinated radical.[32] It is therefore not possible to discern unequivocally between these forms by their electronic spectra alone.

Resonance Raman Spectroscopy. In order to gain further information on characteristic spectroscopic features of coordinated phenoxyl radicals we have measured RR spectra of various electrochemically generated Zn phenoxyl radical complexes in acetonitrile or dichloromethane solutions containing 0.1 M $[N\text{-}(n\text{-butyl})_4]PF_6$. The spectra were recorded at 20 °C by using excitation lines between 413 and 432 nm, coincident with the phenoxyl radical $\pi \rightarrow \pi^*$ transition.

The RR spectrum of $[Zn(L^4)(Me\text{-}acac)]^{\bullet +}$ ($[\mathbf{6}]^{\bullet +}$) shown in Figure 12a displays two prominent bands at 1511 and 1611 cm^{-1} which constitute the characteristic vibrational signature of *para*-substituted phenoxyl radicals[36a,37] and which, in turn, differs significantly from that of the corresponding phenolates.[37] These two bands are readily assigned to the modes ν_{7a} (1511 cm^{-1}) and ν_{8a} (1611 cm^{-1}) which predominantly include the C−O stretching and the $C_{ortho}-C_{meta}$ stretching coordinate, respectively. For the uncoordinated 2,6-di-*tert*-butyl-4-methoxyphenoxyl radical the ν_{8a} mode is found at a substantially lower frequency (1590 cm^{-1}) and with a significantly weaker RR activity.[38] Thus, the RR spectrum confirms the notion that one-electron oxidation of **6** generates a phenoxyl radical ligand, which is coordinated to the Zn ion.

This conclusion is also true for $[Zn(L^4)(Ph_2acac)]^{\bullet +}$ ($[\mathbf{4}]^{\bullet +}$) since its RR spectrum reveals a similar picture (Figure 12b) with two strong bands at 1509 and 1611 cm^{-1}. The slightly lower frequency of the ν_{7a} mode in $[\mathbf{4}]^{\bullet +}$ as compared to $[\mathbf{6}]^{\bullet +}$ results from the effect of the ligand exchange, Ph_2acac^- *vs* Me-acac$^-$, on the coordinated phenoxyl, which should be most sensitively reflected by the ν_{7a} mode. The Ph_2acac^- ligand, which exhibits a strong $\pi \rightarrow \pi^*$ (intraligand) transition at ca. 380 nm, is also the origin of the bands at 1286, 1314, and 1492 cm^{-1} as well as of the weak shoulder at 1600 cm^{-1} in the spectrum of $[\mathbf{4}]^{\bullet +}$, which are preresonance enhanced with 417 nm excitation. The contribution of these bands, relative to those of the phenoxyl radical, is significantly increased in the RR spectrum of $[\mathbf{3}]^{\bullet +}$ (Figure 12c). Due to the blue-shift of the $\pi \rightarrow \pi^*$ phenoxyl transition which overlaps with that of Ph_2acac^-, a selective enhancement of the phenoxyl compared to the Ph_2acac^- modes is not possible. Choosing an excitation line on the high-energy side of the 380 nm $\pi \rightarrow \pi^*$ transition at 351 nm, however, provides a selective enhancement of the RR bands of Ph_2acac^- (Figure 12d). The comparison with the RR spectrum in Figure 12c clearly shows that the only band which can unambiguously be attributed to the phenoxyl radical in $[\mathbf{3}]^{\bullet +}$ is the 1511 cm^{-1} band, whereas the band at 1600 cm^{-1} originates from a Ph_2acac^- mode. This latter band most likely obscures the ν_{8a} phenoxyl mode which, for the *p*-*tert*-butyl-substituted species, is found in the range between 1591 and 1601 cm^{-1} and generally exhibits a relatively weak RR intensity.[38]

(36) (a) Tripathi, G. N. R.; Schuler, R. H. J. Phys. Chem. **1988**, *92*, 5129. (b) Johnson, C. R.; Ludwig, M.; Asher, S. A. *J. Am. Chem. Soc.* **1986**, *108*, 905.

(37) Mukherjee, A.; McGlashen, M. L.; Spiro, T. G. *J. Phys. Chem.* **1995**, *99*, 4912.

(38) Schnepf, R.; Sokolowski, A.; Müller, J.; Bachler, V.; Wieghardt, K.; Hildebrandt, P. *J. Am. Chem. Soc.* Submitted for publication.

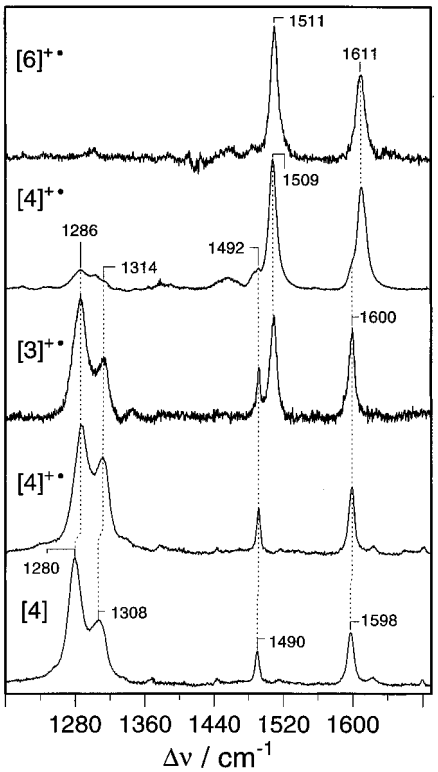

Figure 12. RR spectra of (a) $[\mathbf{6}]^{\bullet+}$ (λ_{exc} = 413 nm); (b) $[\mathbf{4}]^{\bullet+}$ (λ_{exc} = 417 nm); (c) $[\mathbf{3}]^{\bullet+}$ (λ_{exc} = 413 nm); (d) $[\mathbf{4}]^{\bullet+}$ (λ_{exc} = 351 nm); (e) [**4**] (λ_{exc} = 351 nm) measured in CH_3CN solution containing 0.1 M $[N(n\text{-}but)_4]PF_6$, except $[\mathbf{6}]^{\bullet+}$ in CH_2Cl_2.

Finally, it is instructive to compare the RR spectrum of the Ph_2acac^- ligand in $[\mathbf{4}]^{\bullet+}$ with that of the reduced complex [**4**], measured under the same conditions (Figure 12d,e). In $[\mathbf{4}]^{\bullet+}$, all the Ph_2acac^- bands are found at higher frequencies (by 2−7 cm^{-1}) compared to [**4**]. Evidently, the oxidation of the phenolate exerts a subtle influence on the electron density distribution and the structure of the Ph_2acac^- ligand.

The Zn trisphenolato complexes as well as their one-electron oxidation products are involved in acid−base equilibria including $[Zn(L^2)]^-/[Zn(L^2)]^\bullet$, $[Zn(L^2H)]/[Zn(L^2H)]^{\bullet+}$, and $[Zn(L^2H_2)]^+/[Zn(L^2H_2)]^{\bullet 2+}$ (see Scheme 2). We have measured a series of RR spectra from radical complexes in different solvents and in the absence and presence of the proton-accepting base *tert*-butyl oxide; however, none of these species could be obtained in a pure form. Thus, the measured spectra include contributions from all three radical species, $[Zn(L^2H_2)]^{\bullet 2+}$, $[Zn(L^2H)]^{\bullet+}$, and $[Zn(L^2)]^\bullet$, albeit with different relative concentrations. This is most clearly reflected in the ν_{7a} band region (1490−1530 cm^{-1}) as shown by a selection of the spectra in Figure 13.

In order to determine the most relevant spectral parameters of the radicals $[Zn(L^2)]^\bullet$, $[Zn(L^2H)]^{\bullet+}$, and $[Zn(L^2H_2)]^{\bullet 2+}$, *i.e.*, ν_{8a} and ν_{7a}, we have focused onto the spectral range between 1470 and 1650 cm^{-1} by employing a component analysis.[39] This approach takes into account that the frequencies and half widths of the ν_{8a} and ν_{7a} bands of a given species are independent of its relative concentration and the excitation line. In a good approximation, also the ν_{8a}/ν_{7a} intensity ratio can be regarded as constant for the various excitation lines which were employed (418−432 nm). Thus, the eight measured spectra were fitted by a superposition of component spectra rather than of independent bands, as shown in Figure 13. In this fashion, a satisfactory fit for all measured spectra was achieved with an overall error of ±0.5 and ±1.6 cm^{-1} for the frequencies and half widths, respectively, and of 15.5% for the relative intensities.

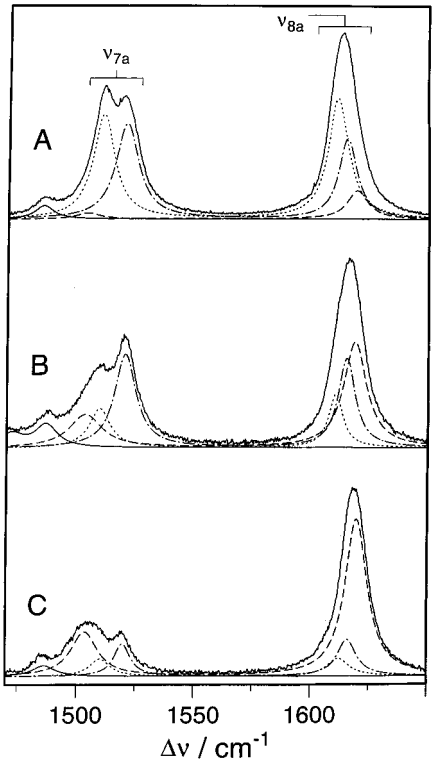

Figure 13. RR spectra of electrochemically generated radical species $[Zn(L^2H_2)]^{\bullet 2+}$, $[Zn(L^2H)]^{\bullet+}$, and $[Zn(L^2)]^\bullet$ in (A) CH_3CN (+ $K[OC(CH_3)_3]$), (B) CH_3CN with $[Zn(L^2H)]$ as starting material, (C) CH_3CN with $[Zn(L^2H_2)]^+$ as starting material. The component spectra of individual species are indicated by the dashed ($[Zn(L^2H_2)]^{\bullet 2+}$), dotted ($[Zn(L^2H)]^{\bullet+}$), and dashed-dotted ($[Zn(L^2)]^\bullet$) lines.

The assignment of the component spectra to the individual species was straightforward by taking into account that $[Zn(L^2H_2)]^{\bullet 2+}$ is the prevailing form in samples prepared from $[Zn(L^2H_2)]^+$ in the absence of added base (Figure 13c), whereas $[Zn(L^2)]^\bullet$ is expected to be the main component in the presence of high base concentrations (Figure 13a,b). The ν_{8a} and ν_{7a} frequencies of the various species obtained are listed in Table 5. The high ν_{8a} frequencies as well as the frequency difference ($\nu_{8a}-\nu_{7a}$) are characteristic for metal-coordinated phenoxyl radicals. On the other hand, the variation of the frequencies, in particular the frequency difference ($\nu_{8a}-\nu_{7a}$), from $[Zn(L^2)]^\bullet$ (95 cm^{-1}) to $[Zn(L^2H)]^{\bullet+}$ (102 cm^{-1}), and $[Zn(L^2H_2)]^{\bullet 2+}$ (115 cm^{-1}) indicates that the stepwise protonation of the phenolates affects the electron distribution in the coordinated phenoxyl.

Attempts to obtain the RR spectrum of the corresponding radical complex derived from [**1**] was aggravated by its significantly lower stability. Thus, it was only possible to detect the ν_{7a} and ν_{8a} modes of $[Zn(L^1H_2)]^{\bullet 2+}$ at 1506 and 1593 cm^{-1}. This indicates that the replacement of the methoxy- by the *tert*-butyl-substituent lowers the ν_{8a} frequency, thereby reflecting a decrease of the $C_{ortho}-C_{meta}$ bond strength.

Discussion and Conclusion

In the present study we have shown that pendent arm macrocycles of the type 1,4,7-tris(2-hydroxybenzyl)-1,4,7-triazacyclononane form stable octahedral complexes with zinc(II). It is possible to reversibly protonate one or two coordinated phenolate groups affording the corresponding coordinated phenols. Protonation weakens the resulting Zn−O(H)R bond with respect to the corresponding Zn−OR bond.

We have established that appropriate bulky substituents at the coordinated phenolate in *ortho* and *para* positions allow a reversible one-electron oxidation of the ligand with formation of stable, coordinated phenoxyl radical ligands.

Table 5. Comparison of RR Spectral Data of Coordinated and Uncoordinated Phenoxyl Radicals

compound	ν_{8a}, cm^{-1}	ν_{7a}, cm^{-1}	$\Delta(\nu_{8a}-\nu_{7a})$, m^{-1}	ref
phenoxyl	1557	1505	52	36a
tyrosyl	1565	1510	55	36b
2,6-di-*tert*-butyl-4-methoxyphenoxyl	1590	1511	79	this work
$[Zn(L^2H_2)]^{\bullet 2+}$	1619	1504	115	this work
$[Zn(L^2H)]^{\bullet +}$	1612	1510	102	this work
$[Zn(L^2)]^{\bullet}$	1615	1520	95	this work
$[Zn(L^1H_2)]^{\bullet 2+}$	1593	1506	87	this work
$[\mathbf{6}]^{\bullet +}$	1611	1511	100	this work
$[\mathbf{4}]^{\bullet +}$	1611	1509	102	this work
$[\mathbf{3}]^{\bullet +}$	not detected	1511		this work

Table 6. Crystallographic Data for **2**, **3**·0.5Toluene·1n-Hexane, and **4**

	2	**3**·0.5Toluene·1n-Hexane	**4**
formula	$C_{42}H_{64}BF_4N_3O_7Zn$	$C_{47.5}H_{69}N_3O_3Zn$	$C_{35}H_{45}N_3O_4Zn$
fw	875.14	795.43	637.11
cryst syst	cubic	monoclinic	monoclinic
space group	$I\,23$	$P2_1/n$	$P2_1/c$
a, Å	20.636(2)	12.118(2)	15.389(3)
b, Å		19.723(3)	11.236(2)
c, Å		19.266(3)	18.449(3)
β, deg		104.23(2)	100.70(3)
V, $Å^3$	8787(2)	4463(1)	3135(1)
Z	8	4	4
ρ_{calc}, g cm^{-3}	1.323	1.184	1.350
F (000)	3712	1716	1352
μ, mm^{-1}	0.627	0.592	0.827
cryst dimens, mm	0.32 × 0.53 × 0.60	0.56 × 0.60 × 0.76	0.14 × 0.07 × 0.21
λ, Å	0.71073	0.71073	0.71073
T, K	173(2)	100(2)	100(2)
no. of total data collected	20073	34664	12243
no. of unique obsd. data	2724	7829	4497
no. of parameters refined	188	493	394
R^a	0.0352	0.048	0.049
largest residual electron density e $Å^{-3}$	0.61	0.51	0.43

[a] $R = \sum(|F_o| - |F_c|)/\sum|F_o|$.

The phenoxyl−zinc complexes exhibit spectroscopic features which allow their unambiguous identification.

(i) Their electronic spectra resemble closely those of uncoordinated phenoxyl radicals. One or two intense absorption maxima in the visible range at ∼400 nm are bathochromically shifted upon coordination and their intensity increases. A third less intense absorption maximum at 500−800 nm is also detectable in the metal ion bound and uncoordinated species.

(ii) The EPR spectra of zinc phenoxyl complexes show that on the time scale of such an experiment the spin of the unpaired electron is delocalized not only over the phenoxyl aromatic ring but also over the metal ion *and* neighboring coordinated phenolates but not over bound phenol ligands. It is conceivable that on the EPR time scale a rapid electron hopping process occurs as shown in eq 5.

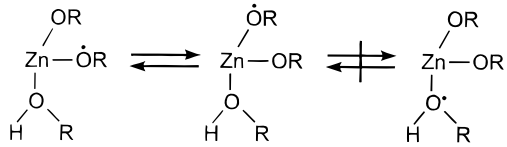

(5)

(iii) RR spectroscopy is a very powerful tool for the identification and characterization of (coordinated) phenoxyl radicals. Upon excitation in resonance with the $\pi \rightarrow \pi^*$ transition of the phenoxyl, the RR bands originating from the modes ν_{7a} (∼1500 cm^{-1}; C−O stretching) and ν_{8a} (∼1600 cm^{-1}; C═C stretching) are clearly detectable. The exact positions of these bands as well as their RR intensity ratio can be used to distinguish between coordinated and uncoordinated phenoxyls. For Zn-coordinated *para*-methoxy-substituted phenoxyls, the ν_{8a} mode is found between 1610 and 1620 cm^{-1}, and the frequency difference ($\nu_{8a}-\nu_{7a}$) is between 95 and 115 cm^{-1}. In these spectra, the RR intensity ratio of the modes ν_{8a} and ν_{7a}, $I(\nu_{8a})/I(\nu_{7a})$, is ≥ 1. In contrast, the uncoordinated radical (2,6-di-*tert*-butyl-4-methoxyphenoxyl) exhibits the ν_{8a} mode at a lower frequency (1590 cm^{-1}), accompanied by a substantial lowering of the RR intensity, *i.e.*, $I(\nu_{8a})/I(\nu_{7a}) < 0.1$, and a decrease of ($\nu_{8a}-\nu_{7a}$) below 80 cm^{-1}. These findings are in line with the RR spectroscopic results obtained from Lippard's complex [Zn(BIDPhe)Cl_2] with an uncoordinated (dangling) phenoxyl arm.[32] These authors only observed the ν_{7a} mode (at the same position as for the free radical BIDPhe), whereas the ν_{8a} band was apparently not detectable. Also, for ribonucleotide reductase (uncoordinated tyrosyl) only the ν_{7a} mode was detected.[40] On the other hand, the RR spectrum of the active form of GO allows the identification of both modes at 1595 (ν_{8a}) and 1487 cm^{-1} (ν_{7a}), corresponding to a frequency difference of 108 cm^{-1}, which is characteristic for a coordinated tyrosyl.[14] This conclusion is also true for the related enzyme glyoxal oxidase, which exhibits an active site similar to GO as reflected, *inter alia*, by the same ν_{8a} and ν_{7a} frequencies.[41]

Experimental Section

Physical Measurements. Electronic spectra were recorded on a Perkin Elmer Lambda 19 (range: 220−1400 nm) or on a Hewlett Pakard HP 8452A diode array spectrophotometer (range: 220−820 nm). Cyclic voltammograms, square wave voltammograms, and

(39) Döpner, S.; Hildebrandt, P.; Mauk, A. G.; Lenk, H.; Stempfle, W. *Spectrochem. Acta* **1996**, *A51*, 573.

(40) Backes, G.; Sahlin, M.; Sjöberg, B.-M.; Loehr, T. M.; Sanders-Loehr, J. *Biochemistry* **1989**, *28*, 1923.

(41) Whittaker, M. W.; Kersten, P. J.; Nakamura, N.; Sanders-Loehr, J.; Schweizer, E. S.; Whittaker, J. W. *J. Biol. Chem.* **1996**, *271*, 681.

coulometric experiments were performed with EG&G equipment (Potentiostat/Galvanostat Model 273A). EPR spectra of complexes (10^{-3} M, CH_3CN/CH_2Cl_2 solutions containing 0.10 M [N(*n*-butyl)$_4$]-PF_6) were measured on a Varian E-9 X-band spectrometer with 100 kHz modulation frequency at 298 K in a quartz cell (d = 0.3 mm). The data were digitized by means of the data station Stelar DS-EPR (Stelar s.n.c., Mede, Italy). The spectra were simulated by iteration of the isotropic hyperfine coupling constants and line widths. We thank Dr. F. Neese (Abteilung Biologie der Universität Konstanz) for a copy of his EPR simulation program. All NMR spectra were recorded on a 400 MHz Bruker AMX series spectrometer.

RR spectra were recorded with a U1000 spectrograph (2400/mm holographic gratings) equipped with a liquid nitrogen-cooled CCD detector (Instruments S.A.). The output of a dye laser (stilbene 3; Coherent 899-01) pumped by an argon ion laser (multiline UV; Coherent Innova 400) served as excitation source. The laser power at the sample was about 50 mW. In order to avoid photoinduced degradation, the sample which exhibits an optical density of *ca.* 1.5 at the excitation wavelength was deposited in a rotating cell. The Raman scattered light was detected at 90° with a scrambler placed in front of the entrance slit of the spectrometer to account for the polarization-sensitivity of the gratings. The spectral slit width was 2.8 cm^{-1}. The spectra, measured with an acquisition time of 15 s, were linearized in wavenumbers yielding an increment of 0.24 cm^{-1} and a total spectral range of *ca.* 200 cm^{-1}. Thus, several spectra covering different but overlapping ranges are combined to give the whole spectra displayed in this work. In these spectra, the contributions of the solvent and the supporting electrolyte are subtracted.

Syntheses. The ligands H_3L^1 and H_3L^2 and their isotopomers deuterated at the benzyl groups have been prepared as described in ref 21.

1,4-Dimethyl-7-(3,5-di-*tert*-butyl-2-hydroxybenzyl)-1,4,7-triazacyclononane (L^3H). To a solution of 2,4-di-*tert*-butylphenol (30 g; 0.145 mol) in methanol (40 mL) was added dropwise with stirring at room temperature a suspension of paraformaldehyde (4.5 g; 0.15 mol) and $LiOH\cdot H_2O$ (0.5 g; 0.012 mol) in methanol (40 mL). The mixture was heated to reflux for 12 h. The solvent was removed by rotary evaporation, and the orange-brown viscous residue was dissolved in n-hexane (20 mL). Upon filtration and storage of the solution at 0 °C for 12 h, a colorless precipitate of 3,5-di-*tert*-butyl-2-hydroxybenzyl alcohol formed (17.5 g; 51%).

The crude product was dissolved in $CHCl_3$ (60 mL), and a solution of PBr_3 (8.1 g; 0.03 mol) in $CHCl_3$ (60 mL) was added dropwise. After stirring the resulting solution for 1 h at 20 °C water (100 mL) was added. The organic phase was quickly washed three times with water and dried over $MgSO_4$, and the solvent was removed by evaporation. The resulting pale-yellow viscous oil crystallized at 0 °C within a few days (3,5-di-*tert*-butyl-2-hydroxybenzyl bromide) (19.5 g; 88%).

To a mixture of 1,4-dimethyl-1,4,7-triazacyclononane (2.0 g; 12.7 mmol) and KOH (1.1 g; 20 mmol) in dry toluene (30 mL) was added dropwise a solution of 3,5-di-*tert*-butyl-2-hydroxybenzyl bromide (3.8 g; 12.7 mmol) in toluene (30 mL). The solution was heated to 70 °C for 6 h. The cooled solution was filtered, and the solvent was removed by rotary evaporation. A yellow-brown viscous oil of the desired ligand L^1H was obtained which was not further purified but used for the preparation of complexes. EI-Ms (pos. Ion) m/z 375 (M^+) calcd for $C_{23}H_{40}N_3O$ 374.6. ^{1}H NMR ($CDCl_3$, 400 MHz): δ 7.18 (d, J = 2.52 Hz, 1H), 6.81 (d, J = 2.52 Hz, 1H), 3.77 (s, 2H), 2.94−2.54 (m, 12H), 2.36 (s, 6H), 1.42 (s, 9H), 1.27 (s, 9H). ^{13}C{^{1}H} ($CDCl_3$, 100 MHz): 154.6, 140.0, 135.4, 123.3, 122.5, 122.0, 62.0, 58.3, 58.0, 53.5, 46.7, 34.8, 34.1, 32.7, 29.6 ppm.

Sodium [1,4-Dimethyl-7-(3-*tert*-butyl-5-methoxy-2-hydroxybenzyl)-1,4,7-triazacyclononane] Na(L^4). A solution of 1,4-dimethyl-1,4,7-triazacyclononane (3.0 g; 19.0 mmol) and paraformaldehyde (0.57 g; 19.0 mmol) in methanol (50 mL) was heated to reflux for 1 h. To the then yellow solution was added 2-*tert*-butyl-4-methoxyphenol (3.42 g; 0.019 mol), and heating to reflux was continued for 12 h. The solvent was removed by rotary evaporation, and the orange-brown viscous residue was dissolved in dry THF. To this solution was added a small amount of NaH (0.46 g; 0.019 mol) (*caution*: very exothermic reaction). The reaction volume was reduced to one-half by evaporation of THF and dry diethyl ether (10 mL) and dry n-pentane (30 mL) were added. A pale-yellow precipitate of Na(L^4) formed (2.75 g; 39%). ^{1}H NMR ($CDCl_3$, 400 MHz): δ 6.76 (d, J = 2.9 Hz, 1H), 6.39 (d, J = 2.9 Hz, 1H), 3.73 (s, 2H), 3.72 (s, 3H), 2.88 (t, 4H), 2.63 (t, 4H), 2.51 (s, 4H), 2.33 (s, 6H), 1.39 (s, 9H) ppm. ^{13}C{^{1}H} ($CDCl_3$, 100 MHz): δ 151.3, 150.8, 137.6, 123.5, 112.2, 111.0, 61.8, 58.2, 57.9, 55.5, 53.7, 46.5, 34.7, 29.3 ppm.

[Zn(L^1H_2)]$BF_4\cdot H_2O$ (1) and [Zn(L^2H_2)]$BF_4\cdot H_2O$ (2). A solution of H_3L^1 or H_3L^2 (1.0 mmol) in acetonitrile (50 mL) and $Zn(BF_4)_2\cdot 4H_2O$ (0.31 g; 1.0 mmol) was heated to reflux for 2 h. From the cooled solution colorless microcrystals precipitated which were filtered off; yield: ∼70%. Anal. Calcd for $C_{51}H_{82}BF_4N_3O_4Zn$: C, 64.2; H, 8.7; N, 4.4. Found: C, 63.4; H, 8.5; N, 4.4. Anal. Calcd for $C_{42}H_{63}BF_4N_3O_7Zn$: C, 57.6; H, 7.2; N, 4.8. Found: C, 58.1; H, 7.3; N, 4.9. The deuterated isotopomers [Zn(d_6-L^1H_2)]$BF_4\cdot H_2O$ (d_6-**1**) and [Zn(d_6-L^2H_2)]$BF_4\cdot H_2O$ (d_6-**2**) were prepared analogously by using the deuterated ligands d_6-H_3L^1 or d_6-H_3L^2 for the synthesis. **1**: ^{1}H NMR (CD_3CN, 400 MHz): δ 7.42 (d, J = 2.28 Hz, 1H); 7.40 (d, J = 2.39 Hz, 2H); 7.12 (d, J = 2.39 Hz, 2H); 7.09 (d, J = 2.28 Hz, 1H); 3.99 (s, 6H); 2.8 (m, 6H); 2.6 (m, 6H); 1.47 (s, 9H); 1.44 (s, 18H); 1.28 (s, 27H) ppm. ^{13}C{^{1}H} NMR (CD_3CN, 100 MHz): δ 152.9, 144.3, 137.4, 127.2, 126.2, 121.6, 60.3, 51.8, 35.5, 35.0, 31.7, 30.9, 30.4 ppm. **2**: ^{1}H NMR (CD_3CN, 400 MHz): δ 6.92 (d, J = 3.04 Hz, 3H); 6.68 (d, J = 3.04 Hz, 3H); 3.89 (s, 6H); 2.7 (m, 6H); 2.5 (m, 6H); 1.46 (s, 21H); 1.41 (s, 6H). ^{13}C{^{1}H} NMR (CD_3CN, 100 MHz): 154.4, 148.8, 139.6, 123.6, 115.4, 114.4, 62.3, 56.2, 51.7, 35.5, 30.7, 30.2 ppm.

[Zn(L^2H)] (2a). To a solution of **2** (0.43 g; 0.5 mmol) in CH_3OH (70 mL) was added KOH (0.10 g; 1.7 mmol) at ambient temperature. Upon stirring for a few minutes a colorless precipitate formed which was collected by filtration and recrystallized from CH_2Cl_2 solution. (0.22 g; 56%). Anal. Calcd for $C_{42}H_{61}N_3O_6Zn$: C, 65.6; H, 8.0; N, 5.5. Found: C, 64.8; H, 8.1; N, 5.4. ^{1}H NMR (CD_2Cl_2, 400 MHz): δ 6.79 (d, J = 3.20 Hz, 3H); 6.44 (d, J = 3.20 Hz, 3H); 4.24 (d, J = 10.78 Hz, 3H); 3.68 (s, 9H); 2.97 (d, J = 10.78 Hz, 3H); 2.62 (m, 6H); 2.05 (m, 6H); 1.46 (s, 27H) ppm. ^{13}C{^{1}H} (CD_2Cl_2, 100 Hz): δ 162.6, 146.8, 136.7, 123.7, 114.9, 114.1, 63.5, 57.1, 56.4, 48.2, 34.9, 30.4 ppm.

Treatment of a solution of **2a** in CD_2Cl_2 (∼10^{-2} M) with 1 equiv of potassium *tert*-butyloxide generates a solution of [Zn(L^2)]$^-$ and *tert*-butylhydroxide. The NMR data of **2a** are as follows: ^{1}H NMR (CD_2Cl_2, 400 MHz): δ 6.80 (d, J = 3.28 Hz, 3H); 6.44 (d, J = 3.28 Hz, 3H); 4.24 (d, J = 10.78 Hz, 3H); 3.68 (s, 9H); 2.97 (d, J = 10.78 Hz, 3H); 2.05−2.62 (m, 12H); 1.46 (s, 27H) ppm. ^{13}C{^{1}H} (CD_2Cl_2, 100 MHz): 162.6, 146.8, 136.7, 123.7, 114.9, 114.1, 63.5, 57.1, 56.5, 48.2, 34.9, 30.4 ppm.

[Zn(L^3)(Ph_2acac)] (3). To a solution of L^3H (0.38 g; 1.0 mmol) in methanol (30 mL) was added $Zn(BF_4)_2\cdot 4H_2O$ (0.31 g; 1.0 mmol). After 30 min of stirring at room temperature K[Ph_2acac] (0.26 g; 1.0 mmol) was added. Within a few hours, a microcrystalline yellow precipitate formed which was collected by filtration and recrystallized from diethyl ether. Recrystallization from a toluene/n-hexane mixture (1:1) produced yellow single crystals of **3**·0.5toluene·1n-hexane. The isotopomer [Zn(d_2-L^3)(Ph_2acac)] was prepared by using d_2-L^3H as starting material. Anal. Calcd for $C_{38}H_{51}N_3O_3Zn$: C, 68.8; H, 7.75; N, 6.3. Found: C, 68.8; H, 7.7; N, 6.3. FAB-MS (MNBA): m/z (rel intensity %) 661 {[Zn(L^3)(Ph_2acac)]$^+$, 55}, 438 {[Zn(L^3)]$^+$, 100}; 663 {[d_2-Zn(L^3)(Ph_2-acac)]$^+$, 55}, 440 {[d_2-Zn(L^3)]$^+$, 100}. ^{1}H NMR ($CDCl_3$, 400 MHz): δ 7.90 (m, 4H); 7.36 (m, 6H); 7.08 (d, J = 2.80 Hz, 1H); 6.73 (d, J = 2.80 Hz, 1H); 6.53 (s, 1H); 4.66 (d, J = 11.54 Hz, 1H); 3.37 (d, J = 11.54 Hz, 1H), 2.80 (s, 3H); 2.42 (s, 3H); 2.12−3.65 (m, 12H); 1.28 (s, 9H); 1.24 (s, 9H) ppm. ^{13}C{^{1}H} ($CDCl_3$, 100 MHz): δ 186.02, 185.28, 166.74, 142.94, 141.70, 136.49, 130.58, 130.01, 129.68, 127.90, 127.86, 127.15, 127.08, 125.52, 123.00, 119.79, 93.09, 64.36, 57.04, 54.42, 54.26, 52.06, 50.34, 47.20, 47.16, 47.13, 35.08, 33.64, 32.02, 29.75 ppm.

[Zn(L^4)(Ph_2acac)] (4). Yellow crystals of **4** were obtained following the procedure given above for **3** by using Na(L^4) as ligand. Yield: 0.25 g (39%). Single crystals for X-ray crystallography were obtained by recrystallization from acetonitrile/water (1:1) mixture. The isotopomer [Zn(d_2-L^4)(Ph_2acac)] was prepared by using [d_2-L^4]Na as starting material. Anal. Calcd for $C_{35}H_{45}N_3O_4Zn$: C, 66.0; H, 7.1; N, 6.6. Found: C, 65.8; H, 7.0; N, 6.6. FAB-MS (MNBA) m/z (rel intensity %) 636 {[Zn(L^4)(Ph_2acac)]$^+$, 35}; 412 {[Zn(L^4)]$^+$, 100}; 637.4 {[Zn(d_2-L^4)(Ph_2acac)]$^+$, 50}; 414 {[Zn(d_2-L^4)]$^+$, 100}. ^{1}H NMR ($CDCl_3$, 400 MHz): δ 7.89 (m, 4H); 7.36 (m, 4H); 6.77 (d, J = 3.20 Hz, 1H); 6.54

(s, 1H); 6.41 (d, J = 3.20 Hz, 1H); 4.64 (d, J = 11.60 Hz, 1H); 3.69 (s, 3H); 3.33 (d, J = 11.60 Hz, 1H); 2.79 (s, 3H); 2.42 (s, 3H); 2.12−3.62 (m, 12H); 1.27 (s, 9H) ppm. $^{13}C\{^1H\}$ ($CDCl_3$, 100 MHz): δ 186.0, 185.6, 164.0, 145.0, 142.9, 141.9, 138.3, 130.0, 129.7, 127.9, 127.8, 127.1, 127.0, 120.0, 114.2, 113.6, 93.2, 64.0, 57.0, 56.5, 54.4, 54.2, 52.0, 50.2, 47.2, 47.1, 47.0, 35.0, 29.5 ppm.

[Zn(L^4)(Ph$_2$acac)]PF$_6$ (5). To a solution of **4** (0.20 g; 0.54 mmol) in dry deoxygenated CH_2Cl_2 was added ferrocenium hexafluorophosphate (0.18 g; 0.54 mmol) under an argon blanketing atmosphere at room temperature. A color change from orange to green was observed. After stirring for 1 h deoxygenated dry diethyl ether (10 mL) was added to the solution. Upon storage of this solution at 0 °C for 1 day a green-brown microcrystalline precipitate formed which was collected by filtration: 0.10 g (24%). μ_{eff} (298 K) = 1.7 μ_B. Anal. Calcd for $C_{35}H_{45}F_6N_3O_4PZn$: C, 53.75; H, 5.80; N, 5.37. Found: C, 53.5; H, 5.8; N, 5.4.

[Zn(L^4)(Me-acac)] (6). A white microcrystalline precipitate of **6** was obtained following the procedure given above for **4** by using Me-acac as ligand. Yield: 0.29 g (55%). Anal. Calcd for $C_{26}H_{43}N_3O_4Zn$: C, 59.3; H, 8.2; N, 8.0. Found: C, 59.2; H, 8.2; N, 8.0. FAB-MS (MNBA) *m/z* (rel intensity %) 527 {[Zn(L^4)(Me-acac)]$^+$, 30}; 527 {[Zn(L^4)]$^+$, 100}. ^1H NMR ($CDCl_3$, 250 MHz): δ = 6.77 (d, J = 3.20 Hz, 1H); 6.36 (d, J = 3.20 Hz, 1H); 4.42 (d, J = 11.49 Hz, 1H); 3.69 (s, 3H); 3.20 (d, J = 11.49 Hz, 1H); 2.52 (s, 3H); 2.39 (s, 3H); 2.10−3.45 (m, 12H); 2.011 (s, 3H); 1.89 (s, 3H); 1.79 (s, 3H); 1.34 (s, 9H) ppm. $^{13}C\{^1H\}$ ($CDCl_3$, 63 MHz): δ = 164.0, 144.0, 138.0, 120.0, 114.3, 113.9, 102.7, 98.4, 77.2, 63.7, 56.8, 56.4, 54.3, 54.1, 51.9, 50.1, 47.5, 47.1, 35.0, 29.4, 28.6, 27.9 ppm.

Crystallography. Details of the crystal data, data collection, and refinement are summarized in Table 6. Intensities and lattice parameters of a colorless crystal of **2**, a pale-yellow crystal of **3**·0.5toluene·1n-hexane, and a pale-yellow crystal of **4** were measured on a Siemens SMART system by using Mo-Kα radiation at 173(2), 100(2), and 100-(2) K, respectively. No corrections for absorption effects were carried out. The structures were solved by conventional Patterson and difference Fourier and direct methods and refined with anisotropic thermal parameters for all non-hydrogen atoms. The Siemens program package SHELXTL PLUS (G. M. Sheldrick, Universität Göttingen) was used throughout. All methyl, methylene, methine, and aromatic hydrogen atoms were placed at calculated positions and were refined with isotropic temperature factors. The function minimized during full-matrix least-squares refinement was $\sum w(|F_o| - |F_c|)^2$.

In the structure of **3**·0.5toluene·1n-hexane both solvent molecules of crystallization were found to be disordered. The toluene molecule lies on a crystallographic center of symmetry, and two positions (1:1) were successfully refined (with an occupancy factor 0.5 for C and H atoms, respectively). The disorder of the n-hexane molecule was also successfully modeled by a split atom model over three positions with occupancy factors given in the Supporting Information.

Acknowledgment. We thank the Fonds der Chemischen Industrie for financial support. P.H. thanks the Deutsche Forschungsgemeinschaft for granting a Heisenberg fellowship. We also thank a reviewer for his constructive criticism and valuable suggestions.

Supporting Information Available: Tables of crystallographic data and structure refinement data, atom coordinates and U_{eq}, bond lengths and angles, anisotropic thermal parameters, and calculated positional parameters of hydrogen atoms for **2**, **3**·0.5toluene·1n-hexane, and **4** and figures of the resolved static disorder in **2** and of the resolved disorder of solvent molecules in **3** (23 pages). See any current masthead page for ordering and Internet access instructions.

JA970417D